Non-invasive *in vivo* quantification of the developing optical properties and graded index of the embryonic eye lens using SPIM

LAURA K. YOUNG[1,2,4], MIGUEL JARRIN[2,3,4], CHRISTOPHER D. SAUNTER[1,2], ROY QUINLAN,[2,3,5] AND JOHN M. GIRKIN[1,2,6]

[1]*Department of Physics, Durham University, South Road, Durham, DH1 3LE, UK*
[2]*Biophysical Sciences Institute, Durham University, South Road, Durham, DH1 3LE, UK*
[3]*Department of Biosciences, Durham University, Upper Mountjoy, Stockton Road, Durham, DH1 3LE, UK*
[4]*Joint first authors* [5]*r.a.quinlan@durham.ac.uk* [6]*j.m.girkin@durham.ac.uk*

Abstract: Graded refractive index lenses are inherent to advanced visual systems in animals. By understanding their formation and local optical properties, significant potential for improved ocular healthcare may be realized. We report a novel technique measuring the developing optical power of the eye lens, in a living animal, by exploiting the orthogonal imaging modality of a selective plane illumination microscope (SPIM). We have quantified the maturation of the lenticular refractive index at three different visible wavelengths using a combined imaging and ray tracing approach. We demonstrate the method can be used with transgenic and vital dye labeling as well as with both fixed and living animals. Using a key eye lens morphogen and its inhibitor, we have measured their effects both on lens size and on refractive index. Our technique provides insights into the mechanisms involved in the development of this natural graded index micro-lens and its associated optical properties.

OCIS codes: (330.5370) Physiological optics; (330.7324) Visual optics, comparative animal models; (170.1420) Biology; (170.2520) Fluorescence microscopy

References and links

1. T. M. Greiling and J. I. Clark, "Early lens development in the zebrafish: a three-dimensional time-lapse analysis," Dev. Dynam. **238**(9), 2254–2265 (2009).
2. S. R. J. Easter and G. N. Nicola, "The development of eye movements in the zebrafish (danio rerio)," Dev. Psychobiol. **31**(4), 267–276 (1997).
3. D. T. Clark, "Visual responses in developing zebrafish," Ph.D. thesis, University of Oregon (1981).
4. R. D. Fernald, "The optical system of fishes," in "The visual system of fish," R. H. Douglas and M. B. A. Djamgouz, eds. (Chapman and Hall, (1990)), pp. 45–61.
5. J. Piatigorsky, "Lens differentiation in vertebrates. a review of cellular and molecular features." Differentiation **19**(3), 134–153 (1981).
6. C. Slingsby, G. J. Wistow, and A. R. Clark, "Evolution of crystallins for a role in the vertebrate eye lens," Protein Sci. **22**(4), 367–380 (2013).
7. L. Gunhaga, "The lens: a classical model of embryonic induction providing new insights into cell determination in early development," Philos Trans R Soc Lond B Biol Sci. **366**(1568), 1193–1203 (2011).
8. F. J. Lovicu, J. W. McAvoy, and R. U. de Longh, "Understanding the role of growth factors in embryonic development: insights from the lens." Philos Trans R Soc Lond B Biol Sci. **366**(1568), 1204–1218 (2011).
9. B. P. Madakashira, D. A. Kobrinski, A. Hancher, E. C. Arneman, B. D. Wagner, F. Wang, H. Shin, F. J. Lovicu, L. W. Reneker, and M. Robinson, "Frs2α enhances fibroblast growth factor-mediated survival and differentiation in lens development," Development **139**(24), 4601–4612 (2012).
10. D. Upadhya, M. Ogata, and L. W. Reneker, "Mapk1 is required for establishing the pattern of cell proliferation and for cell survival during lens development," Development **140**(7), 1573–1582 (2013).
11. Q. Xie, R. MCGreal, R. Harris, G. C. Y, L. W, L. W. Reneker, Musil, L. S, and A. Cvekl, "Regulation of c-maf and αA-crystallin in ocular lens by fibroblast growth factor signalling," J. Biol. Chem. **291**, 3947–3958 (2016).
12. Y. Verma, K. D. Rao, M. K. Suresh, H. S. Patel, and P. K. Gupta, "Measurement of gradient refractive index profile of crystalline lens of fisheye in vivo using optical coherence tomography," Appli. Phys. B, **87**, 607–610 (2007).
13. H. Zhao, P. H. Brown, M. T. Magone, and P. Schuck, "The molecular refractive function of lens γ- crystallins," J. Mol. Biol. **411**(3), 680–699 (2011).
14. M. Bahrami, M. Hoshino, B. Pierscionek, N. Yagi, J. Regini, and K. Uesugi, "Optical properties of the lens: an explanation for the zones of discontinuity," Exp. Eye Res. **124**, 93–99 (2014).

15. M. Jarrin, L. Young, W. Wu, J. M. Girkin, and R. A. Quinlan, "In vivo, ex vivo and in vitro approaches to study intermediate filaments in the eye lens," Methods Enzymol. **568**, 581–611 (2016).
16. J. Huisken, J. Swoger, F. Del Bene, J. Wittbrodt, and E. H. K. Stelzer, "Optical sectioning deep inside live embryos by selective plane illumination microscopy," Science **305**(5686), 1007–1009 (2004).
17. L. Godinho, J. S. Mumm, P. R. Williams, E. H. Schroeter, A. Koerber, P. S. W., S. D. Leach, and R. O. Wong, "Targeting of amacrine cell neurites to appopriate synaptic laminae in the developing zebrafish retina," Development **132**(22), 5069–5079 (2005).
18. C. E. Jones and J. M. Pope, "Measuring optical properties of an eye lens using magnetic resonance imaging." Magn. Reson. Imaging **22**(2), 211–220 (2004).
19. J. Birkenfeld, A. de Castro, S. Ortiz, D. Pascual, and S. Marcos, "Contribution of the gradient refractive index and shape to the crystalline lens spherical aberration and astigmatism." Vis. Res. **86** (2013).
20. J. Birkenfeld, A. de Castro, and S. Marcos, "Astigmatism of the ex vivo human lens: Surface and gradient refractive index age-dependent contributions." Invest. Ophthalmol. Vis. Sci. **56**(9), 5067–5073 (2015).
21. M. Hoshino, K. Uesugi, N. Yagi, S. Mohri, J. Regini, and B. Pierscionek, "Optical properties of in situ eye lenses measured with x-ray talbot interferometry: a novel measure of growth processes." PLoS ONE **6**(9), e25140 (2011).
22. J. M. Taylor, C. D. Saunter, G. D. Love, J. M. Girkin, D. J. Henderson, and B. Chaudry, "Real-time optical gating for three-dimensional beating heart imaging," J. Biomed. Opt. **16**(11), 1–8 (2011).
23. C. Bourgenot, C. D. Saunter, J. M. Taylor, J. M. Girkin, and G. D. Love, "3D adaptive optics in a light sheet microscope," Opt. Express **20**(12), 13252–13261 (2012).
24. K. Watanabe, Y. Nishimura, T. Oka, T. Nomoto, T. Kon, T. Shintou, M. Hirano, Y. Shimada, N. Umemoto, J. Kuroyanagi, Z. Wang, Z. Zhang, N. Nishimura, T. Miyazaki, T. Imamura, and T. Tanaka, "In vivo imaging of zebrafish retinal cells using fluorescent coumarin derivatives," BMC Neurosci., **11**(116), 1–12 (2010).
25. D. M. Parichy, M. R. Elizondo, M. G. Mills, T. N. Gordon, R. E. Engeszer, "Normal table of postembryonic zebrafish development: staging by externally visible anatomy of the living fish," Dev. Dyn., **238**, 2975âĂŞ-3015 (2009).
26. C. B. Kimmel, W. W. Ballard, S. R. Kimmel, B. Ullmann, T. F. Schilling, "Stages of embryonic development of the zebrafish," Dev. Dyn., **203**(3), 253âĂŞ-310 (1995).
27. G. Streisinger, C. Walker, N. Dower, D. Knauber, F. Singer, "Production of clones of homozygous diploid zebra fish (Brachydanio rerio)," Nature **291**(5813), 293âĂŞ-296 (1981).
28. S. van der Walt, S. C. Colbert, and G. Varoquaux, "The numpy array: A structure for efficient numerical computation," Comput. Sci. Eng. **13**(2), 22–30 (2011).
29. C. E. Shannon and W. Weaver, *The Mathematical Theory of Communication* (University of Illinois Press, 1949).
30. T. M. Cover and J. A. Thomas, *Elements of Information Theory* (John Wiley & Sons, New York, 1991).
31. K. D. Rao, Y. Verma, H. S. Patel, and P. K. Gupta, "Non-invasive ophthalmic imaging of adult zebrafish eye using optical coherence tomography," Curr. Sci. India **90**(11), 1506–1510 (2006).
32. V. Fleisch and S. C. F. Neuhauss, "Visual behavior in zebrafish," Zebrafish **3**(2), 1–11 (2006).
33. S. Barnes and R. A. Quinlan, "Small molecules, both dietary and endogenous, influence the onset of lens cataracts." Exp. Eye. Res. **156**, 87–94 (2016).

1. Introduction

The zebrafish eye lens is a biological micro-lens that starts to form 16 hours post fertilization (hpf) [1] via a complex physical, chemical and biological process. As the lens grows its refractive power develops, focusing light onto the photoreceptor layer of the retina from about 3 days post fertilization (dpf) [2], leading to a visual (opto-kinetic) response by 4 dpf [3]. In order to achieve these optical properties, the radius of curvature must be matched by the appropriate refractive index relative to the humours of the anterior and posterior chambers for light to be focused onto the retina. The optical power of the fish lens has to be higher than those of land animals because the cornea, being immersed in water, has minimal effective optical power [4]. As the lens grows during development, so its radius of curvature increases and this would lower its refractive power. However, the refractive index (RI) increases during lens development as a result of the expression of lens crystallins [5, 6]. The RI and its gradient are determined by biological signals. For example, fibroblast growth factor (FGF) is one essential both to lens development and lens cell differentiation [7–10]. FGF-signaling also determines the optical properties of the lens by regulating crystallin expression [11].

In the adult zebrafish eye lens, as with all vertebrate lenses, there is a non-uniform RI profile that is higher in the center and lower at the periphery [12]. Such a gradient refractive index (GRIN) lens is made from living cells and their expressed lens crystallins. The unique amino acid

composition and high concentration of these proteins generate the local RI [6, 13, 14]. A GRIN can reduce optical aberrations compared to a uniform RI lens of the same shape. In a spherical fish lens, a uniform RI would cause peripheral rays to be focused at a shorter distance than paraxial rays, causing significant spherical aberration. The zebrafish counters this by producing a GRIN lens. This can be manipulated experimentally [15].

We use a selective plane illumination microscope (SPIM [16]) to image refractive changes directly in both living, and fixed, zebrafish lens from 2 to 4 dpf. We relate these measurements to changes in the diameter of the lens and its focal length. The refraction of the SPIM light sheet by the eye lens can be observed directly via light emission from surrounding fluorescent molecules. We have developed an integrated image analysis and ray tracing method to determine the RI of small lenses using the fluorescence images obtained with a SPIM. To visualize the refracted light sheet, there must be fluorescence in the volume after the optical element. In the zebrafish, this can be achieved by either genetic manipulation or by vital fluorescent dyes. We measured the refractive power of transgenic (Q01; [17]), fluorescent fish lenses with and without the addition of membrane-staining vital dyes (Coumarin 6 and BoDIPY TMRE). We use our technique to quantify the effective RI and the RI gradient in normal lenses in the developing zebrafish. We additionally show measureable changes in the effective RI associated by manipulating the FGF-signalling pathway.

Our new, non-invasive method makes no assumptions concerning water distribution as required for NMR [18] and some OCT measurements [19], where lens extraction is also required [20, 21]. We make direct ray tracing measurements on lenses in living animals, which therefore allows for modulators of eye development to be studied *in vivo*. This will assist the development of new therapies for eye diseases (e.g. cataracts or presbyopia) and also accelerate future optical innovations using nano-structured materials to build artificial micro-lenses and their composites.

Methods

Selective plane illumination microscopy (SPIM)

Measurements were made with a custom-built SPIM [22, 23]. The illumination source is a four wavelength (405, 488, 561 and 632 nm) fibre-coupled laser (Stradus Versalase, Vortran) and is collimated with a 13 mm focal length achromatic lens (AC0604-013-A-ML, Thorlabs). The light is passed through a 4f relay on to a cylindrical lens (ACY254-050-A, Thorlabs) to produce a sheet focus, which is projected on to the back aperture of the 0.3 NA 10x (illumination) objective lens (CFI Plan Fluor 10xW, Nikon) via a second 4f relay. Chromatic focus shift created by the illumination optics is compensated by movement of the final relay lens. The light sheet excites a plane of fluorescence within the sample. Fluorescence emission is imaged along an axis perpendicular to the direction of propagation of the light sheet, via a 0.8 NA 16x (imaging) objective lens (CFI75 LWD 16xW, Nikon) to collimate the light and an imaging lens (AC254-150-A-ML, Thorlabs) to re-focus it. Fluorescence (or bright field) light is imaged through the appropriate filter by a camera with $6.45\,\mu\text{m} \times 6.45\,\mu\text{m}$ pixels and a resolution of 1392×1040 pixels (QI Click Mono, 01-QICLICK-R-F- M-12, QImaging).

Sample preparation

This technique requires a fluorescent label in the tissue after the eye lens to visualize the subsequent focusing of the excitation light. For this study we tested Q01 transgenic zebrafish, which express cyan fluorescent protein (CFP) fused to a membrane-targeting sequence of the Gap43 gene under the control of Pax6 enhancers, ensuring expression in the eye. This transgenic line was developed by the laboratory of Rachel O. L. Wong (University of Washington, Seattle [17]). All animal procedures conformed to the Statement of the EU Directive 2010/63/EU for animal experiments. Q01 fish were additionally labeled with Coumarin 6, a spatially-restricted membrane-staining

vital dye [24] and BoDIPY TMRE, a general plasma membrane fluorescent label, to demonstrate the extension of this technique to the study of wild-type animals as well as other transgenic lines that do not express fluorescent protein in and around the eye.

Q01 fertilized eggs were collected, cleaned, and washed with egg water (E3 saline solution for zebrafish eggs and embryos) within 1 hpf. Fertilized eggs were pooled and then placed in a sterile Petri dish containing egg water and incubated at a temperature of 28.5 °C. At 4 hpf, 1-phenyl 2-thiourea (PTU) was added to each dish to a final concentration of 30 μg/ml in order to reduce the formation of melanocytes. A control group was produced and showed no significant difference in eye size at either 1 or 2 dpf associated with the PTU treatment. After 24 hpf embryos that were to be used to study the FGF pathway were incubated overnight with FGF2 (Invitrogen, final concentration 250 ng/mL) or SU5402 (Invitrogen, final concentration 5 μM). Controls were taken from the same clutch as the sample groups in order to minimize inter-clutch variability, although variability between individuals from each clutch is inherent to Zebrafish embryonic/larval development [25–27]. Before imaging, the zebrafish embryos were dechorionated and placed in egg water and, if required, a vital dye was added [15]. When vital dyes were used fish were incubated for two hours with 0, 5.7, 17.1, or 34.2 μM Coumarin 6 and/or with 100 μM BoDIPY TMRE. To increase uptake of these dyes 1 % (v/v) dimethyl sulfoxide was also added. Prior to imaging these embryos, they were washed twice in egg water. Although our procedure allows an individual embryo to be tracked over time, in this study we used embryos at the stated developmental stages, timed from the point of fertilization [26]. This approach minimized potential variations due to repeated anesthesia and handling of the embryos. We also demonstrate that measurements can be made in fixed animals. Zebrafish were fixed in 4 % (w/v) formaldehyde and a sample taken at 2, 3 and 4 days of development.

Imaging protocol

In each experimental condition and at each age we tested six eyes from three different zebrafish embryos. Immediately before imaging, the zebrafish were anaesthetized with tricaine (MS-222, Sigma Aldrich Stock), which was diluted in egg water to a final concentration of 0.2 mg/mL. The embryos were held in this solution within a piece of fluorinated ethylene propylene (FEP) tubing, which has a refractive index (n = 1.344) that is closely matched to that of water (n = 1.333). Embryos were placed in a custom-built SPIM [22, 23] and aligned such that the light sheet passed parallel to the optical axis of the eye (Fig. 1). This was achieved by rotating the embryo such that the center of the eye lens to be imaged is in the same plane as the light sheet using the brightfield image as a guide. This was done to ensure consistency in the incidence angle between the light sheet and the optical axis of the eye. A sequence of images (planes, each separated by 1 μm) were taken through the entire volume of the eye lens to be imaged and located closest to the incoming illumination. The plane through the center of the lens to be measured was manually selected afterwards by an experienced operator and was used for image analysis. The center of the lens can be identified as the plane that has the largest apparent lens diameter and contains the central cluster of lens fiber cells. An area containing the lens and an area behind it up to three lens diameters (but not including the second eye) was used for analysis (Fig. 1). Light emission from within the lens to be measured forms part of the image. We observe this fluorescence light via part of the eye lens lying between the plane of the light sheet and the imaging objective. This causes a small amount of refraction of the imaged light, which we corrected for by ray tracing along the imaging z-axis (see Section 2). When imaging the right eye, the embryo was oriented with its left-right axis parallel to the light sheet and with the camera on the ventral side (Fig. 1(a)). The left eye was imaged by rotating the embyro 180 ° about the anteroposterior axis, such that the camera was on the dorsal side with the left eye closest to the illumination objective. The ten-times magnification of the imaging part of the SPIM (a combination of the 16x imaging objective and a 200 mm tube lens) gave an effective pixel size of 0.7 μm in the sample, which

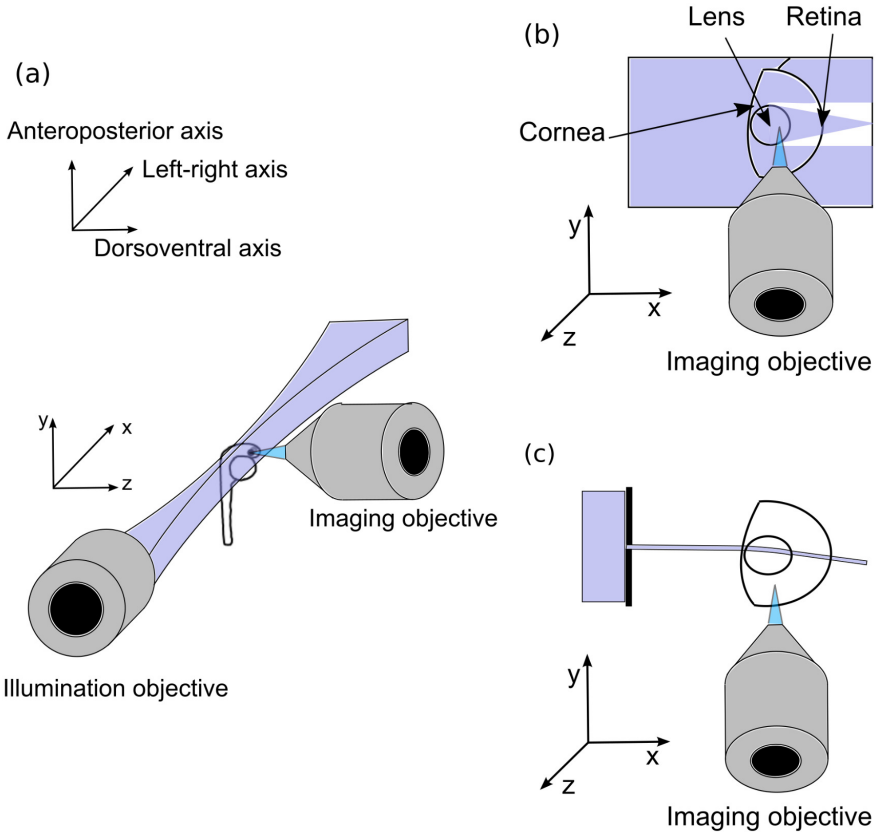

Fig. 1. Alignment of the zebrafish embryo within the SPIM system. (**a**) The axes of the zebrafish embryo showing the left-right axis, which we align parallel to the light sheet (purple shading), and the anteroposterior axis, about which we rotate the embryo. The axes of the light sheet are also shown indicating direction of propagation along x and the optical axis of the imaging objective (blue shading), z. (**b**) A rotated version of (**a**) showing the propagation of the light sheet through the eye of the zebrafish embryo and its subsequent focusing. The light sheet is refracted by the eye lens as indicated. This is observed via the fluorescence signal in the surrounding tissue. Additional refraction by the second (right-most) eye lens is not considered and our analysis does not include light that has passed through it. (**c**) The same as (**b**), but indicating the GRIN measurement procedure, where a pencil beam is selected using a slit aperture.

was verified using a calibration sample comprising 8 μm diameter fluorescent beads embedded in 2% (w/v) agarose gel.

Measurements were usually taken using an excitation wavelength of 405 nm and fluorescence emission from Coumarin 6 was observed through a GPF emission bandpass filter. In experiment (i) we tested six eyes from three transgenic (Q01) zebrafish embryos for each of three concentrations of Coumarin 6 and a control in which no dye was added (we observed the CFP emission only), at each of ages 2, 3 and 4 dpf (total of 36 embryos). In experiment (ii) we demonstrated that the technique can be used with multiple excitation wavelengths with the addition of another dye, BoDIPY TMRE. In this experiment we tested a different set of six eyes from three transgenic embryos at each of 2, 3 and 4 dpf (total of 9 embryos), repeating the measurement with each of the excitation wavelengths (405, 488 and 561 nm). We ensured that the incident light sheet was collimated by imaging a sample of fluorescent dye (Rhodamine 6G) and observing shadows cast within it caused by small imperfections in the FEP tubing. We did this for each excitation wavelength to account for chromatic aberrations present in the SPIM system itself. The shadows cast have no effect on the focal length measured within a zebrafish eye. In experiment (iii) we demonstrated the application of this technique to the study of lens growth by making focal length measurements in embryos in which the FGF pathway had been perturbed. We tested six eyes from three transgenic zebrafish embryos at each of 2, 3 and 4 dpf for each of three conditions: no treatment (control), FGF-signaling inhibition (treatment with SU5402), or FGF-signaling activation (treatment with FGF2) (total of 27 embryos). For each experiment (i-iii) controls were taken from the same clutch as the sample groups, but variability between individuals in each clutch is well documented [25–27]. Finally, in experiment (iv) we demonstrated an extension of the technique by measuring the RI gradient. This was done by tracing narrow vertical sections (mimicking ray bundles) of the light sheet through the eye lens. These measurements were taken in embryos that had been fixed in paraformalydehyde, one fish at each of ages 2, 3 and 4 dpf.

2. Image analysis

The incident light in the SPIM is focused in one axis, but is collimated in the other, producing a narrow sheet (**Fig. 1a**). Introduction of a specimen with optical power affects the propagation of the light sheet, most noticeably refracting the collimated rays in a plane parallel to the sheet. This effect is observed in the fluorescent molecules excited by the refracted light sheet, as shown in **Figs. 1b** and **1c**, and hence the optical power of the eye lens can be deduced from the captured fluorescence image. The effective focal length of the lens was determined by comparison between the fluorescence image and a geometric ray tracing simulation, as summarized in **Fig. 2**.

Image analysis for a uniform refractive index model

The fish lens is spherically symmetric and so we restricted the ray trace to a single plane through the center of the lens, which we modeled as a disk of uniform refractive index, surrounded by water (n = 1.333). Ray tracing and image analysis code was implemented with the Python programming language and Numpy array library [28].

The position of the lens in a single fluorescence image was first measured manually along with its radius, the diameter of the whole eye, and the relative position of the photoreceptor layer in the retina. Using these parameters, the trajectory of parallel rays incident upon the front surface of the lens were traced through the lens. The resulting refracted rays were then rasterized to create a map of expected fluorescence excitation (**Fig. 2a**). Gaussian blur was added to the raster to reduce the presence of aliasing effects. As is apparent from the fluorescence images, the density of fluorophores varies within a sample due to the presence and spacing of different structures, creating intensity variations in the fluorescence after the lens. To account for this, a density map of fluorophores was approximated by measuring the intensity along a narrow section from the center of the lens to the edge of the image. As the eye is approximately radially symmetric, this

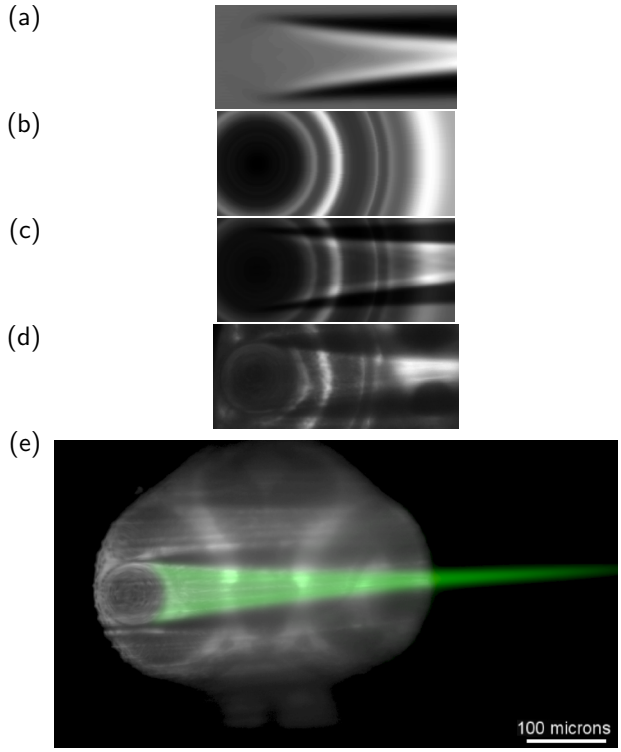

Fig. 2. The method used to measure the focal length of the zebrafish eye lens, using a 2 dpf embryo as an example. (**a**) The fluorescence excitation map derived by rasterizing a geometric ray trace, which modeled the lens as a disk of uniform RI, and then adding Gaussian blur to minimize aliasing artifacts in the bitmap image generation. (**b**) The density map of fluorophors in the sample simulated by a radial projection of the intensity profile derived from the fluorescence image. (**c**) the multiplication of (**a**) and (**b**) then the addition of (**b**) multiplied by a background value to simulate out-of-plane and scattered fluorescence. (**d**) The original fluorescence image that was compared to the simulated image (**c**) and the difference minimized using the Nelder-Mead simplex algorithm to find the optimal RI to use in the ray trace. (**e**) An overlay of the simulated image (in green), computed using the optimal RI in the steps shown in (**a**) - (**c**), which are the simulated images, on the original fluorescence image. The area of the simulated image has been extended to the focal point, although in practice the area containing the second eye is not used. In this immature lens the focal point is far beyond the corresponding retina, and in this case, outside of the embryo.

intensity profile was projected radially from the position of the center of the lens (Fig. 2(b)). This can be considered to simulate the fluorescence image that would be formed if the light sheet were not refracted by the eye lens. We note that the radial symmetry assumed within the zebrafish eye might not be valid outside of the eye, depending on the anatomy and cell structures that are labeled with the fluorophore. However, for the fluorophores we tested this projection reasonably approximates the layered nature of the labeling we observe behind the eye.

The simulated image was created by multiplying the fluorescence excitation map (Fig. 2(a)) by the fluorophore density map (Fig. 2(b)) and a background signal was added to account for delocalized signal arriving from any out-of-plane fluorescence. Comparisons were made between this image (Fig. 2(c)) and the original fluorescence image (Fig. 2(d)) in an area that included the lens and the area after it, up to, but not including, the second eye. The fluorescence emission passes through the portion of the eye lens between the light sheet and the imaging objective and is thus refracted. We use a second ray trace along the imaging axis to account for this small refractive aberration. These angular deviations were used to transform the original image, using coordinate mapping, to estimate the fluorescence image without the effects of this refraction on the emitted light. This transformed image was then compared to the simulated image. In practice we found refraction of this emitted light had a negligible effect on the estimated refractive index, which was mainly driven by fluorescence emission in the area after the eye lens. The free parameters of our model were the center of the lens, the angle of the light sheet, the radius of the lens and the RI. Initial estimates of the lens center and the radius were derived from a manual measurement. Then the free parameters were adjusted to minimize an error metric comparing our model and the experimental image using the Nelder-Meade simplex method. The effective focal length was calculated using the ball lens equation,

$$f = \frac{nR}{2(n-1)}, \tag{1}$$

where R is the radius of the lens and n is the ratio of the refractive index of the lens (n_{lens}) to the refractive index of its surroundings, in this case water ($n_{water} = 1.333$).

For the minimization metric we chose to use the inverse of the mutual information [29, 30] between the simulated and fluorescence images, which were matched in their number of pixels, as this gave the most robust convergence. The Nelder-Meade algorithm uses a given set of starting parameters and generally finds a nearby local minimum. In order to converge on the global minimum, the starting parameters must be sensibly estimated. The starting values for the position of the center of the lens and the radius of the lens were restricted to within 10 pixels of the manually estimated position. The initial ray angles were estimated from a subset of images to be within 10 degrees of the optical axis. The starting values for the refractive index were chosen such that the minimum refractive index was that of water (n = 1.333) and the algorithm was constrained to only test values above this. The maximum starting values for the refractive index were chosen for each age condition based on a manual study of a subset of images and fell within the range $1.333 < n < 1.550$. While the initial values of the free parameters were constrained, values outside of this range (except for the minimum refractive index of 1.333) were allowed during convergence of the algorithm. The optimum value obtained for the RI showed a small variation with the randomly selected initial values. We measured this effect by testing the algorithm ten times on one data set each time using a different randomly selected set of initial values. The standard error of the mean of ten repeated measurements of the RI was less than 0.015.

We verified the accuracy of the RI estimation algorithm using a BK7 glass ball lens (04VQ06, Comar). This lens could not be placed within the SPIM FEP sample chamber, but was instead suspended in a custom-made, 3D printed transparent holder that was filled with a solution of fluorescein. Fluorescence excitation of the fluorescein solution was achieved with a 488 nm laser projected vertically downward through the ball lens. The algorithm described in Section 2 was

used to extract the uniform refractive index of the ball lens, and this was found to be 1.526 ± 0.008 based on four repeated tests on the same image. This is in good agreement with the RI of BK7 Schott glass at 488 nm (1.522).

Image analysis for a gradient RI model

To measure the RI gradient in the zebrafish eye lens we used a slit aperture to restrict the light sheet to a narrow vertical section (Fig. 1(c)). This allowed us to examine narrow ray bundles passing through various vertical positions in the lens and, importantly, to separate paraxial and peripheral rays. Being spherical, the fish lens should introduce positive spherical aberration, focusing peripheral and paraxial rays differently. However, a gradient RI can introduce negative spherical aberration if the RI is lower at the edge of the lens than the center, as typical for most animal lenses. This counteracts the morphologically-induced positive spherical aberration. Additionally, observation of narrow bundles of rays passing through the lens allows us to observe curvature of those ray paths, indicative of a RI gradient.

The technique outlined above was expanded to use a summation of images corresponding to six ray bundles equally spaced across the lens as shown in Fig. 5(a). Whilst a similar effect could be achieved with a single image using a 6-aperture mask in place of the slit, this method provides more flexibility. This was achieved by placing a 40 μm wide slit aperture in the SPIM, at the first conjugate focal plane before the illumination objective. Translating this slit vertically allowed selection of a narrow section of the light sheet, which had a Gaussian intensity profile in the z-axis with a full-width-half-maximum of 3.5 μm in the sample. We modified our ray tracer to use ray bundles, the position and width of which were selected from the summed image. The eye lens was modeled as a gradient refractive index of the form,

$$n(r) = \sum_{i=0}^{3} A_i r^{2i}, \tag{2}$$

where r is the normalized lens radius. The same procedure was followed, as described earlier, with the gradient index coefficients, A_i, the lens radius, the position of the center of the lens and the angle of the light sheet as free parameters in the model.

3. Results and discussion

We used our technique to assess the change in refractive index, lens diameter and the ratio of the effective focal length of the eye to the distance from the center of the lens to the photoreceptor layer in the retina at 2, 3, and 4 dpf in six zebrafish eyes (three fish for each condition). It is apparent from the standard errors of the means in Fig. 3(a)-(d) that the results calculated in experiment (i) with different dye concentrations are in good agreement with each other and with the controls. We therefore conclude that the addition of Coumarin 6 did not significantly affect either lens size or RI. The lens radius increases during development (Fig. 3(a)) as does the RI (Fig. 3(b)), although the latter changed the most between 3 and 4 dpf. The measured effective RIs are close to previous effective RI measurements (n = 1.43) [31] and in the range of RI gradient measurements (n = 1.54 at the center and n = 1.36 at the edge) [12] made in adult zebrafish lenses using optical coherence tomography, but at a longer wavelength (840 nm).

The distance between the lens and the retina increases as the eye grows and so the lenticular focal length must also increase with age. The ratio of the effective focal length to the distance to the photoreceptor layer in the retina from the center of the lens is a measure of this optical function. Optimally this ratio should equal one. It is apparent that this ratio decreases and tends to a value of one at approximately 4.5 dpf (Fig. 3(d)) when vision is optimized in zebrafish [2, 32]. For the first time we present direct imaging of the development of the optical properties of the eye lens in live fish over this critical developmental period.

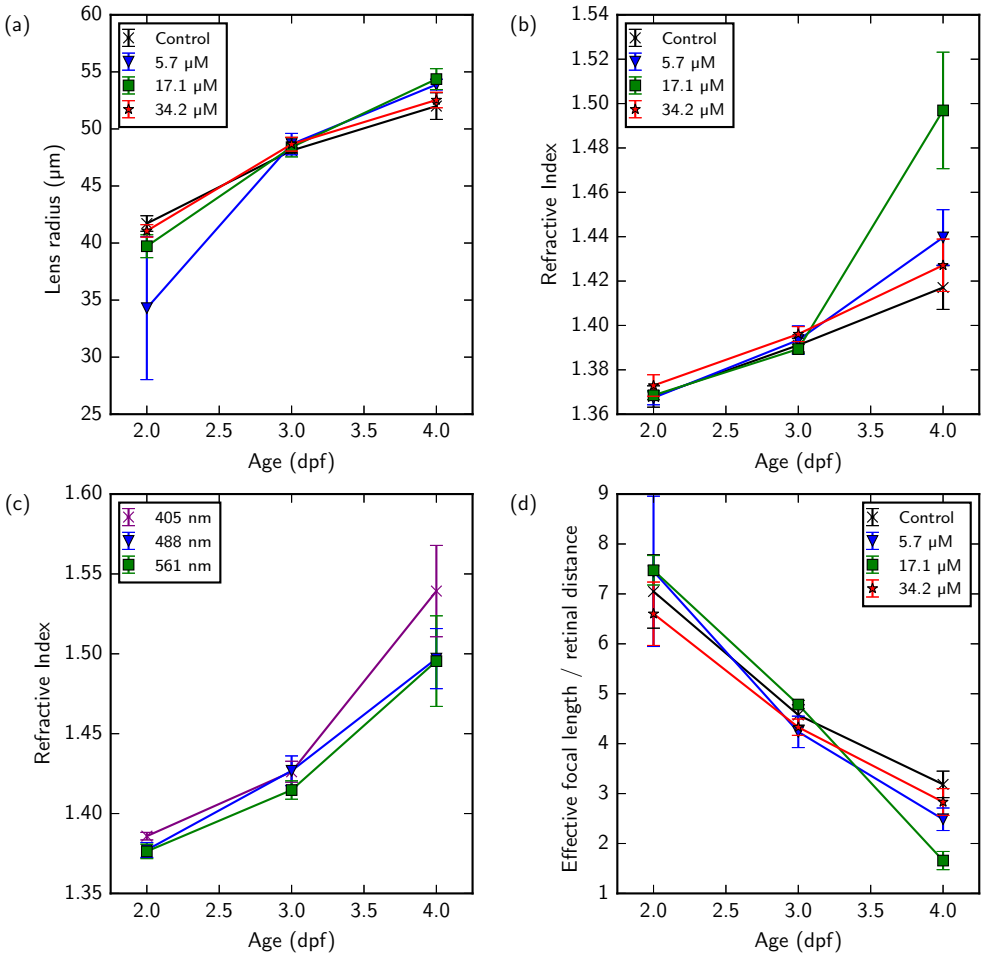

Fig. 3. Zebrafish lens development from day 2 to 4 dpf. **(a)** The increase in radius of the zebrafish eye lens for three final concentrations of Coumarin 6 (5.7, 17.1 and 34.2 μM and a control condition (no Coumarin 6). (**b**) The effective RI of the zebrafish lens, which develops most rapidly between 3 and 4 dpf, for the same concentrations of Coumarin 6. (**c**) The RI of the zebrafish lens measured at three excitation wavelengths using both Coumarin 6 (17.1 μM) and BoDIPY TMRE (100 μM) as fluorescent markers. Chromatic aberration is not detectable in the lenses of these embryos. (**d**) The ratio of the effective focal length, for three concentrations of Coumarin 6 and control, of the zebrafish lens to the distance between the center of the eye lens and the photoreceptor layer in the retina. This ratio should equal one if the eye were focusing appropriately on to the retina. Error bars represent the standard error of the mean from six measurements and the labels in panels (**a**), (**b**) and (**d**) refer to the concentration of Coumarin 6 used to measure the focal length with 405 nm excitation light. We note that different clutches were used in experiment (i) (panels (**a**), (**b**) and (**d**)) and experiment (ii) (panel (**c**). Variability is arises from small developmental differences within the same clutch [25–27], in particular in panel (**b**) the increased RI with 17.1 μm Coumarin 6 at 4 dpf is largely driven by a single outlier (RI=1.62).

In experiment (ii) we repeated the imaging procedure using excitation wavelengths of 405, 488, and 561 nm to explore chromatic dispersion effects. We used a different clutch of eggs to collect these data and so there are small developmental differences that preclude a direct comparison to the data in Figs. 3(a), (b) and (d). The RI measurements made at three separate wavelengths were the same, within the standard errors of the means (Fig. 3(c)). In experiment (iii)

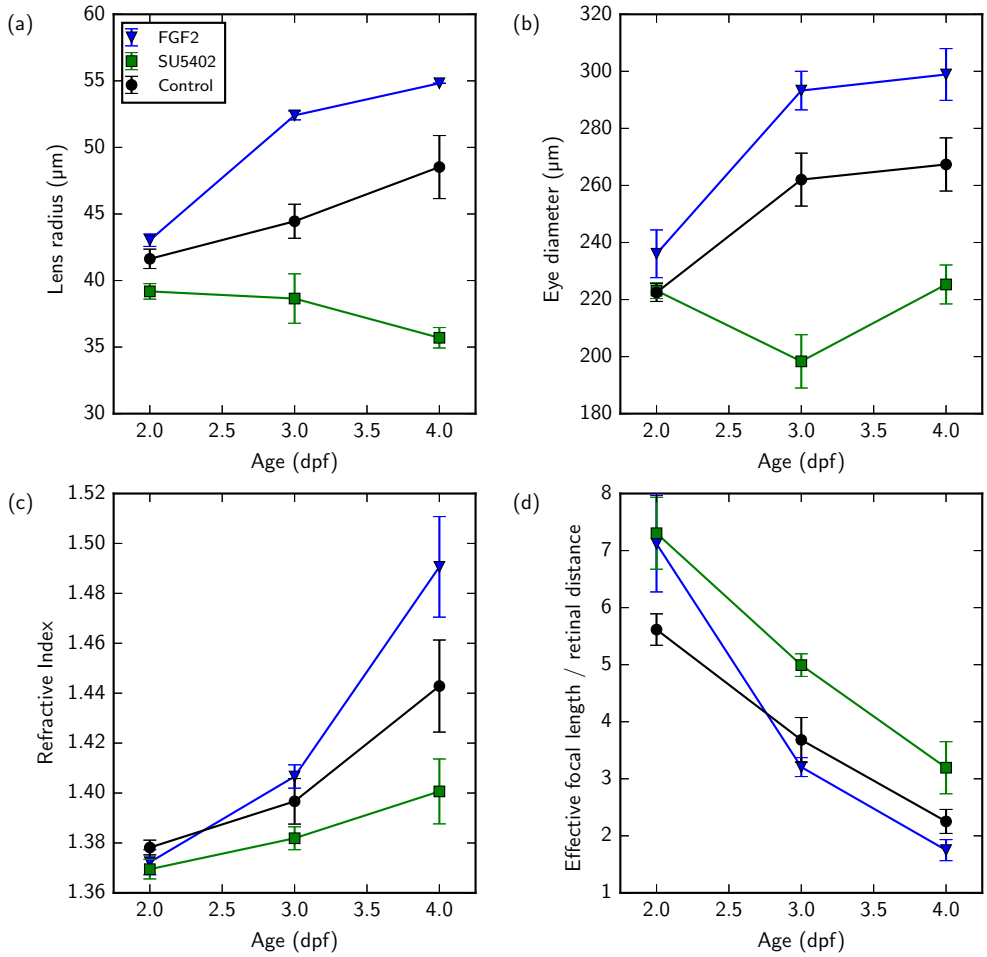

Fig. 4. FGF2 mediated effects upon zebrafish lens development. Zebrafish were exposed to either increased FGF2 concentrations or to a small molecule inhibitor of FGF-signaling, SU5402. Animals from the same clutch were used as controls. (**a**) The change in the radius of the zebrafish lens and (**b**) the change diameter of the zebrafish eye, measured across its widest part. Both of these measurements show a significant reduction in the dimensions of the eye when the FGF pathway is inhibited and a significant increase in these dimensions when this pathway is further activated. (**c**) The effective RI of the zebrafish lens and (**d**) the ratio of the effective focal length of the zebrafish lens to the distance between the center of the lens and the photoreceptor layer in the retina. SU5402 decreased the RI, whilst FGF2 increased the RI relative to controls. A minimum of five independent measurements were made for each data point. Error bars represent the standard error of the mean.

we modulated eye growth and lenticular refractive properties using an FGF-inhibitor (SU5402)

and an FGF-receptor activator (FGF2). Again, these data were collected from a different clutch of eggs to those in the previous experiments, and so a control condition is included for comparison, accounting for small developmental differences between clutches. FGF2 strongly affected lens radius (Fig. 4(a)-(b)), increasing both the eye and lens diameters, whilst SU5402 inhibited this increase, as expected. The RI was also affected by both FGF2, which increased it, and SU5402, which decreased it (Fig. 4(c)). The optical function (focal length/distance to the photoreceptors) was also different for both FGF2 and SU5402 treated zebrafish compared to controls, becoming apparent from 3 dpf onwards. Combined, these data indicate an effect on the development of the lens focal length (Fig. 4(d)) that was driven more strongly by the change in lens size than by the refractive index.

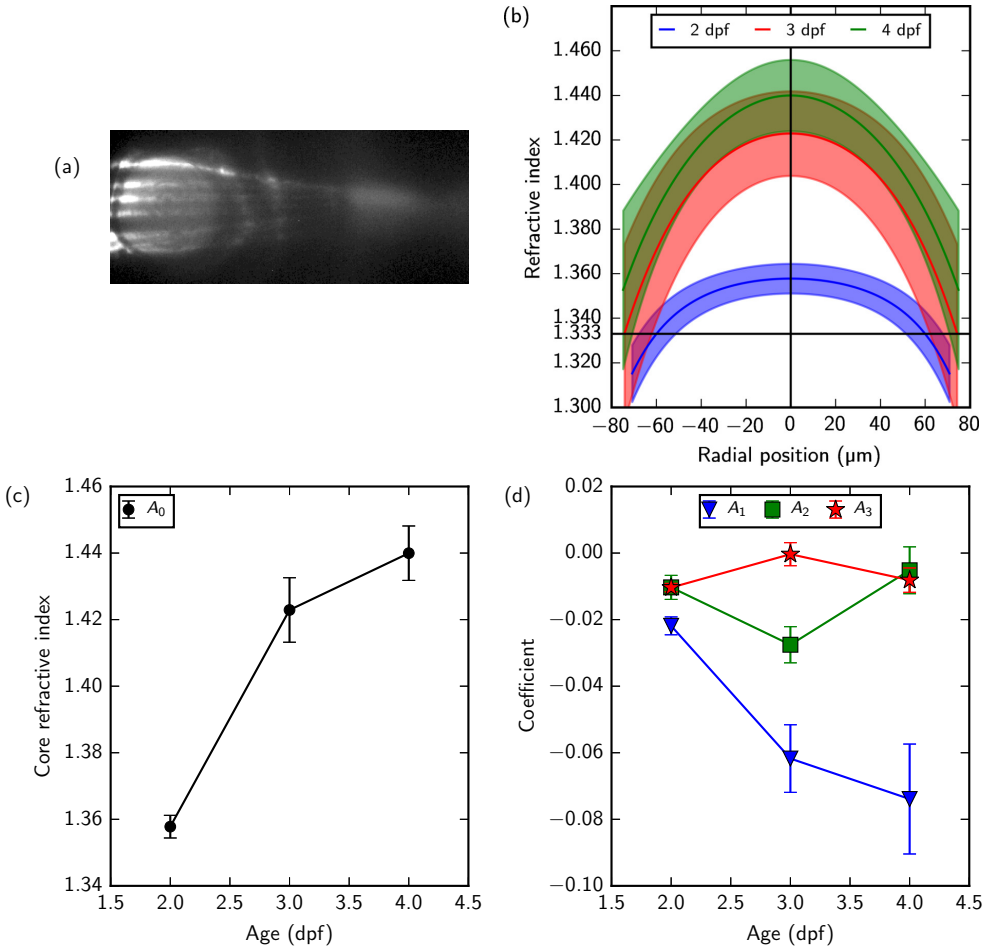

Fig. 5. Measurement of the RI gradient of the zebrafish eye lens. (**a**) An example (a 2 dpf zebrafish) of the average of six images, each of which was recorded for a different position of the aperture placed approximately 12 μm apart. This was used for the image comparison and parameter optimization. (**b**) The RI profile measured for a 2, 3, and 4 dpf zebrafish fixed in paraformaldehyde. The coloured bands and the error bars indicate the 95 % confidence limits on the measurement of the RI profile from a single image (i.e. a single zebrafish eye), determined by repeating the optimization algorithm ten times. (**c**) The development of the RI in the core of the eye lens and of (**d**) the coefficients A_{1-3} with age.

In experiment (iv) we demonstrated that the RI profile of the zebrafish eye lens changes during development (Fig. 5(b)). Figure 5(c) shows that the RI of the lens increases and importantly **Fig. 5d** shows that the radial dependence of the RI also changes, resulting in a steeper gradient with age. Even at 2 dpf a measurable RI gradient is already established. Previous measurements on adult zebrafish show a GRIN starting at 1.36 and increasing to 1.54 at the lens core [12], whereas our measurements for embryonic fish lenses show a lower core RI at this stage of development. This is the first time that GRIN maturation during lens development has been observed and measured in embryos of a living vertebrate. Lens development and visual acuity is critical to zebrafish embryo survival as it must catch prey at 5 dpf when its yolk supply is exhausted.

4. Conclusion

Our technique was developed using zebrafish and we have measured changes in both the radius and the refractive power of the lens throughout development in living transgenic zebrafish embryos with and without the addition of a vital dye and at multiple wavelengths.

We have measured the changes to the radius and RI of the lens when FGF-signaling is altered. Our method makes direct ray tracing measurements in living animals and therefore allows for modulators of eye development to be studied *in vivo* over time, which will assist the development of new therapies for eye diseases [33]. Gene editing strategies [15] can be used to manipulate the GRIN properties of the lens by changing crystallin expression [13] and its short-range order [6]. Using our SPIM-based method we can now study this process in detail to open up the potential of biological regulators to modulate the optical power of a developing micro-lens. By understanding how the optical properties of living micro-lenses are formed, maintained and scaled, the longer term goal of applying biomimetic manufacturing to GRIN lenses for the next generation of miniature sensing and imaging systems will be realized.

Funding

The authors wish to acknowledge funding from the Leverhulme Trust (RPG-2012-554).

Acknowledgements

We would like to thank Rachel O. L. Wong for developing the transgenic fish.

Disclosures

The authors declare that there are no conflicts of interest related to this article.